



Eblabla, A., Li, X. , Alathbah, M., Wu, Z., Lees, J. and Elgaid, K. (2019) Multi-channel AlGaIn/GaN lateral Schottky barrier diodes on low-resistivity silicon for sub-THz integrated circuits applications. *IEEE Electron Device Letters*, 40(6), pp. 878-880.  
(doi:[10.1109/LED.2019.2912910](https://doi.org/10.1109/LED.2019.2912910))

There may be differences between this version and the published version. You are advised to consult the publisher's version if you wish to cite from it.

<http://eprints.gla.ac.uk/198591/>

Deposited on: 02 October 2019

Enlighten – Research publications by members of the University of  
Glasgow

<http://eprints.gla.ac.uk>

# Multi-channel AlGaIn/GaN Lateral Schottky Barrier Diodes on Low Resistivity Silicon for Sub-THz Integrated Circuits Applications

A. Eblabla, X. Li, M. Alathbah, Z. Wu, J. Lees and K. Elgaid

**Abstract**— This work presents novel multi-channel RF lateral Schottky-barrier diodes (SBDs) based on AlGaIn/GaN on Low Resistivity (LR) ( $\sigma = 0.02 \Omega \cdot \text{cm}$ ) silicon substrates. The developed technology offers a reduction of 37 % in onset voltage,  $V_{ON}$  (from 1.34 to 0.84 V), and 36 % in ON-resistance,  $R_{ON}$  (1.52 to 0.97  $\Omega \cdot \text{mm}$ ) as a result of lowering the Schottky barrier height,  $\phi_n$ , when compared to conventional lateral SBDs. No compromise in reverse-breakdown voltage and reverse-bias leakage current performance was observed as both multi-channel and conventional technologies exhibited  $V_{BV}$  of ( $V_{BV} > 30$  V) and  $I_R$  of ( $I_R < 38 \mu\text{A}/\text{mm}$ ), respectively. Furthermore, a precise small-signal equivalent circuit model was developed and verified for frequencies up to 110 GHz. The fabricated devices exhibited cut-off frequencies of up to 0.6 THz, demonstrating the potential use of lateral AlGaIn/GaN SBDs on LR silicon for high-efficiency high-frequency Integrated Circuits applications.

**Index Terms**— GaN, RF diodes, lateral Schottky barrier diode, sub-THz applications, fin-FET, GaN on silicon.

## I. INTRODUCTION

Due to the superior electrical properties of III nitride semiconductors, lateral AlGaIn/GaN Schottky-barrier diodes (SBDs) grown on LR silicon substrates are emerging as a promising device technology for fast switching speed, high-power, low-cost and compact-size communications and radar applications, such as mixers, frequency multipliers, detectors and tunable filters operating at millimeter wave frequencies [1] [2]. GaN-based SBDs with low onset voltage ( $V_{ON}$ ), high reverse-breakdown ( $V_{BV}$ ) voltage, and low reverse-current leakage ( $I_R$ ), high-switching speed ( $R_{ON}$ ) and high cutoff frequency ( $f_c$ ) are essentially required to compete with current III-V technologies [3]. Conventional GaN-based SBD DC and RF performance is still limited to their large  $V_{ON}$ , switching loss and RF leakage when utilizing LR Si substrates. Several

researchers have recently proposed low  $V_{ON}$  along with low  $I_R$  and high  $V_{BV}$  technologies, including recessed anode, dual-filed plates, regrowth cathodes, and dual-channel field-effect rectifier (LFER) [4] [5] [6]. However, these approaches require accurate control of anode etching to the 2DEG and a complicated fabrication process, which incorporates reliability issues and extra processing cost. Nevertheless, a 3-D SBDs integrated with a tri-gate MOS structure has shown outstanding DC characteristics at the expense of RF performance owing to the inherently large junction capacitance ( $C_j$ ) and series resistance ( $R_s$ ) [7]. Therefore, these techniques are only limited to low-frequency applications. To date, most of the research effort into GaN-based SBDs on silicon is predominantly focused on power electronics, with limited literature targeting RF operation. However, achieving high  $f_c$  while maintaining low  $I_R$  and superior  $V_{BV}$  remains a challenge [1].

In this letter, an optimized multi-channel RF AlGaIn/GaN SBDs on LR Si structure is demonstrated using a cost-effective (GaN on LR Si) which is fully compatible with III-V THz monolithic integrated circuit (THz-MIC) technology. In contrast to conventional SBDs, the newly developed devices significantly enhanced the turn-on characteristics, switching loss, ideality factor ( $\eta_n$ ) and  $f_c$ , where a  $V_{ON} = 0.84$  V,  $R_{ON} = 0.97 \Omega \cdot \text{mm}$ ,  $V_{BV} > 30$  V,  $\eta_n = 1.69$  and  $f_c = 0.6$  THz were achieved. This attributes to the direct contact of Schottky anode to 2DEG at the sidewalls of the multi-mesa trenches along with proper design geometries to suppress substrate coupling effects.

## II. DEVICE DESIGN AND FABRICATION

Fig. 1 indicates a cross-section of the fabricated AlGaIn/GaN SBDs on LR Si using a multi-channel structure, which was simultaneously fabricated with conventional SBDs on the same substrate to allow precise comparison. A combination of multi-mesa and T-shaped structures was adopted to form the anode to reduce Schottky barrier height and anode resistivity, respectively. The height ( $H_F$ ), width ( $W_F$ ), spacing ( $S_F$ ) and length ( $L_F$ ) of the nanowires were  $\sim 50, 41, 89$  nm and 2  $\mu\text{m}$ , respectively. The Anode length ( $L_A$ ) and anode head length ( $L_{AH}$ ) were 0.550  $\mu\text{m}$  and 1.1  $\mu\text{m}$ , respectively, whereas the junction length ( $L_j$ ) was 4.28  $\mu\text{m}$ . The total physical anode

Manuscript received January 16, 2019; revised April 6, 2019; accepted April 14, 2019. This work was supported by the Engineering and Physical Sciences Research Council under Grants EP/N014820/2 and EP/P006973/1.

A. Eblabla, M. Alathbah, Z. Wu, J. Lees and K. Elgaid are with the School of Engineering, Cardiff University, Cardiff, CF24 3AA, UK. (email: eblablaa@cardiff.ac.uk).

X. Li is with the School of Engineering, The University of Glasgow, Glasgow, G12 8LT, UK.

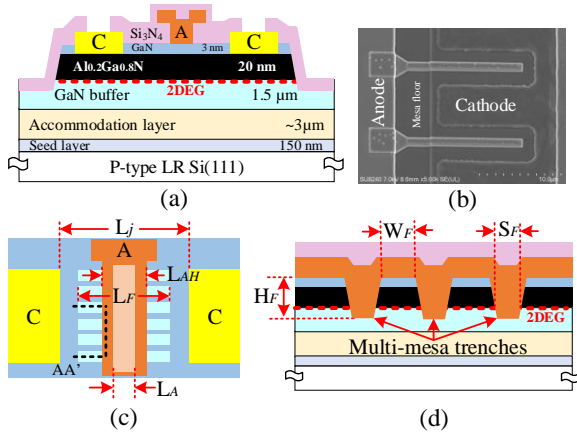


Fig. 1: (a) Cross-sectional view, (b) Scanned-electron microscope (SEM) image and (c) Top-view of the multi-channel SBDs. (d) Cross-sectional representation of the tri-anode along line AA'.

width was  $2 \times 10 \mu\text{m}$ , while the effective anode width for the fin-like anode structure was  $2 \times 5.829 \mu\text{m}$ .

The epitaxy material used in this work was grown on LR Si (111) ( $\sigma = 0.02 \Omega\cdot\text{cm}$ ) provided by Nexperia. The epilayer consists of  $4.65 \mu\text{m}$  buffer,  $20 \text{ nm}$   $\text{Al}_{0.2}\text{Ga}_{0.8}\text{N}$  barrier and  $3 \text{ nm}$  GaN cap layer. A sheet carrier density of  $5.9 \times 10^{12} \text{ cm}^{-2}$  and electron mobility of  $1713 \text{ cm}^2/\text{Vs}$  are determined using Hall measurements. The device fabrication started with defining the Ti/Pt markers, followed by the deposition of Ti/Al/Ni/Au ohmic contacts and rapid thermal annealing at  $790 \text{ }^\circ\text{C}$  in  $\text{N}_2$  environment to form the cathode. Next, a  $\sim 150 \text{ nm}$  depth mesa isolation was performed through  $\text{Cl}_2/\text{Ar}$ -based inductively-coupled plasma (ICP). Then, multi-mesa trenches were defined by e-beam lithography and subsequently etched using  $\text{Cl}_2/\text{Ar}$ -based ICP with an etch depth of  $\sim 50 \text{ nm}$ . A  $100 \text{ nm}$   $\text{Si}_3\text{N}_4$  passivation layer was then deposited using a low-stress inductively-coupled plasma chemical vapour deposition (ICP-CVD) at room temperature. To form the T-shaped anode, E-beam lithography was used to define anode-foot trenches through the  $\text{Si}_3\text{N}_4$  passivation layer using a low-damage  $\text{SF}_6/\text{N}_2$  gas mixture reactive-ion etching (RIE), which was followed by Ni/Au metal stack evaporation to finish the T-shaped anode. Windows in the  $\text{Si}_3\text{N}_4$  at the cathode areas were etched prior to the deposition of Ti/Au bond pads and  $160 \text{ nm}$   $\text{Si}_3\text{N}_4$  layer as a final passivation layer. Device fabrication was finalized by  $\text{Si}_3\text{N}_4$  etching in the measurement pad regions. SEM image of the fabricated devices is shown in Fig. 1b.

### III. RESULTS AND DISCUSSION

#### A. DC Characteristics

Fig. 2 indicates the typical  $I$ - $V$  characteristics of the fabricated conventional and multi-channel structures at room temperature using both linear and logarithm scales. The diode current (A/mm) and resistance ( $\Omega\cdot\text{mm}$ ) of conventional and multi-channel structures are normalized by the total physical anode width ( $2 \times 10 \mu\text{m}$ ) and effective anode width ( $2 \times 5.829 \mu\text{m}$ ), respectively. Fig. 2a reveals that incorporating a multi-channel anode structure reduced  $V_{ON}$  from  $1.34$  to  $0.84 \text{ V}$

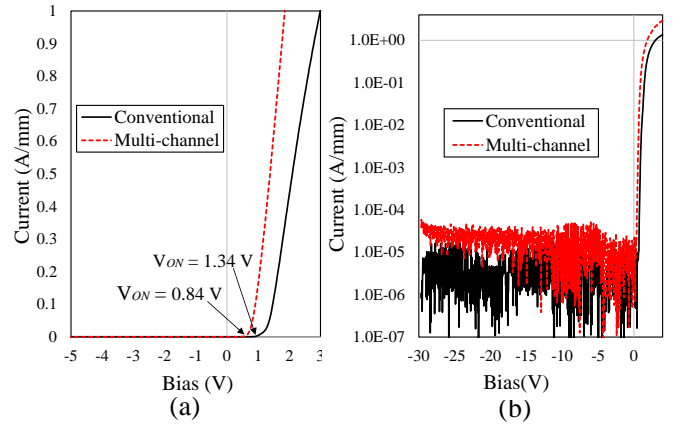


Fig. 2:  $I$ - $V$  characteristics of a fabricated SBD plotted in (a) Linear and (b) Logarithm scale.

together with improved  $R_{ON}$  from  $1.52$  to  $0.97 \Omega\cdot\text{mm}$ . This attributes to the direct anode contact to the 2DEG, where the anode is wrapped around the narrow AlGaIn/GaN bodies.

To further analyze these findings, the semilog  $I$ - $V$  plot (shown in Fig. 2b) is used, which allows the extraction of  $\eta_n$  and  $\phi_n$  based on the analytical equations indicated in [8]. Both device structures exhibited  $\eta_n$  between 1 and 2, which indicates the presence of conduction mechanism besides a thermionic emission mechanism [9]. An improvement of  $14.28 \%$  in  $\eta_n$  (from  $1.97$  to  $1.69$ ) was obtained by the developed multi-channel structure as compared to conventional SBDs. Furthermore, the observed reduction in  $V_{ON}$  when using the new structure corresponds to a reduction of  $17.5 \%$  in  $\phi_n$  (from  $0.78$  to  $0.64 \text{ eV}$ ). However,  $I_R$  was slightly increased with the multi-channel structure, where  $I_R < 38 \mu\text{A}/\text{mm}$  was performed at a reverse voltage of up to  $30 \text{ V}$ . This attributes to the additional anode length where the anode is in direct contact to the GaN buffer in the multi-mesa floor regions. The achieved results are comparable to that of SBDs on semi-insulating (SI)-SiC with recessed anode and regrowth cathode technologies, with better  $V_{BV}$  and  $I_R$  [1]. This enhancement is mainly attributed to the scale of anode-to-cathode spacing and the use of T-shaped anode, owing to the reduction in peak electric field of Schottky junction [5].

#### B. RF Characteristics

On-wafer small-signal  $S$ -parameters measurements were performed in the frequency range  $0.1$  to  $110 \text{ GHz}$  using an Agilent PNA network analyzer (E8361A) and frequency extenders (N5260A). The system was calibrated with an off-wafer calibration impedance standard substrate (ISS), using a Short-Open-Load-Thru (SOLT) calibration technique.

Fig. 3a shows the extracted small-signal circuit model of the devices, which was validated by the good agreement between modelled and measured  $S$ -parameters up to  $110 \text{ GHz}$ , as shown in Fig. 3b. This allows the extraction of SBD intrinsic elements; junction resistance ( $R_j$ ),  $C_j$  and  $R_s$ , which used to determine  $f_c$  of the fabricated devices. As indicated in Fig. 3a, unlike SI-substrates, substrate parasitics ( $S_{sub}$  and  $R_{sub}$ ) are incorporated into the standard SBD circuit model when considering lossy Si

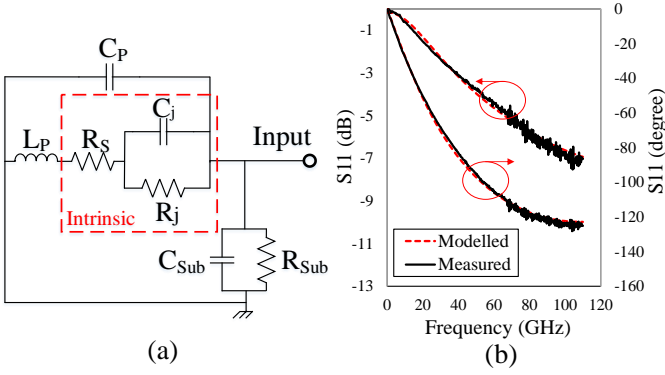


Fig. 3: (a) Schematic of the proposed small-signal equivalent circuit model and (b) measured versus modelled  $S$ -parameters of the fabricated multi-channel AlGaIn/GaN SBDs on LR Si at 0 V bias.

Table I  
EXTRACTED PARAMETERS FOR THE EQUIVALENT CIRCUIT MODEL FOR THE FABRICATED LATERAL SBDs AT 0 V BIAS.

SBD structure	Intrinsic			Extrinsic			
	$C_j$ (fF)	$R_s$ ( $\Omega$ )	$R_j$ (k $\Omega$ )	$L_p$ (pH)	$C_p$ (fF)	$C_{sub}$ (fF)	$R_{sub}$ (k $\Omega$ )
Conventional	49.1	44.9	11.6	40.3	26.4	3.1	10.3
Multi-channel	46.4	51.9	11.6				

as a substrate. Furthermore,  $C_p$  and  $L_p$  represents pad parasitics. However, the external parasitic elements have a significant influence on the model at frequencies beyond 20 GHz.

Table I shows the extracted circuit element values of conventional and multi-channel structures at 0 V bias. In contrast to conventional SBDs, an increase in  $R_s$  by 15.6 % (44.9 to 51.9  $\Omega$ ) and a slight reduction in  $C_j$  by 5.5 % (from 49.1 to 46.4 fF) were observed for the newly developed fin-type technology. This attributes to the additional anode length in the multi-mesa trenches and reduction in  $\phi_n$ , respectively. In addition, the low value of  $C_{sub}$  and high value of  $R_{sub}$  indicates that substrate coupling effect could be neglected in both design structures. This was a result of the proper design geometries where the anode-to-cathode separation (2.415  $\mu\text{m}$ ) is less than the buffer thickness (4.65  $\mu\text{m}$ ) [10].

The extracted values of  $C_j$  as a function of the applied voltage of the fabricated devices are shown in Fig. 4a. It can be seen that  $C_j$  was inversely proportional to the applied reverse voltage, where a sharp drop in  $C_j$  was obtained when changing the voltage from 0 to -2 V. Furthermore, owing to the direct anode contact to 2DEG for multi-channel SBDs,  $C_j$  was significantly reduced at reverse biases beyond -2 V, as compared to conventional SBDs. This reflected a dramatic enhancement in  $f_c$  which can be calculated from  $R_s$  and  $C_j$  [1]. Therefore,  $f_c$  was improved by 32.7 % (from 0.457 to 0.607 THz), as shown in Fig. 4b. However, the achieved  $f_c$  of the fabricated lateral SBDs on LR Si is still limited to their larger  $R_s$ , which mainly depends on material growth quality and cathode contact resistivity, as compared to SBDs realized on GaN-on-Si-SiC substrates [1].

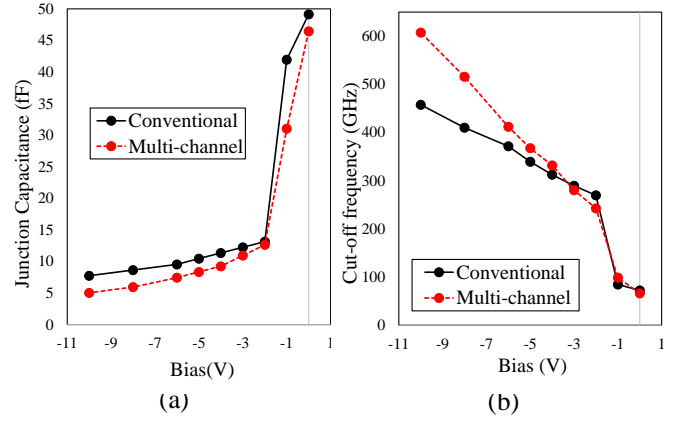


Fig. 4: Junction capacitance ( $C_j$ ) versus voltage, and (b) Cut-off frequency ( $f_c$ ) versus voltage of the fabricated conventional and multi-channel SBDs.

#### IV. CONCLUSION

A newly developed multi-channel RF lateral AlGaIn/GaN SBD on LR Si technology has been realized in this work. A  $V_{ON}$  of 0.84 V along with  $R_{ON}$  of 0.97  $\Omega\cdot\text{mm}$  and  $\eta_n$  of 1.69 were achieved as a result of the direct Schottky anode contact to the 2DEG resulting in a  $\phi_n$  of 0.64 eV. The fabricated devices exhibited  $V_{BV}$  of greater than 30 V along with  $I_R$  of less than 38  $\mu\text{A}/\text{mm}$ . In addition, a newly proposed small-signal circuit model was introduced up to 110 GHz. An  $f_c$  of 0.6 THz at a reverse bias of -10 V was achieved as a result of the optimized SBD design structure and geometries. These findings enable an effective pathway for the realization of high-performance sub-THz-MIC topologies.

#### V. REFERENCES

- [1] K. Shinohara, D. C. Regan, Y. Tang, A. L. Corrión, D. F. Brown, J. C. Wong, J. F. Robinson, H. H. Fung, A. Schmitz, T. C. Oh, S. J. Kim, P. S. Chen, R. G. Nagele, A. D. Margomenos, and M. Micovic, "Scaling of GaN HEMTs and Schottky Diodes for Submillimeter-Wave MMIC Applications," in *IEEE Transactions on Electron Devices*, vol. 60, no. 10, pp. 2982-2996, Oct. 2013. DOI: 10.1109/TED.2013.2268160.
- [2] T. Boles and G. Lopes, "GaN Schottky diodes for RF wireless power detection and conversion," *2015 European Microwave Conference (EuMC)*, Paris, 2015, pp. 1003-1006. DOI: 10.1109/EuMC.2015.7345935.
- [3] B. Ren, M. Liao, M. Sumiya, L. Wang, Y. Koide, and L. Sang, "Nearly ideal vertical GaN Schottky barrier diodes with ultralow turn-on voltage and on-resistance," in *Applied Physics Express*, vol. 10, no. 5, pp. 051001, March 2017. DOI: 10-7567/APEX.10.051001.
- [4] Y. Lian, Y. Lin, J. Yang, C. Cheng and S. S. H. Hsu, "AlGaIn/GaN Schottky Barrier Diodes on Silicon Substrates With Selective Si Diffusion for Low Onset Voltage and High Reverse Blocking," in *IEEE Electron Device Letters*, vol. 34, no. 8, pp. 981-983, Aug. 2013. DOI: 10.1109/LED.2013.2269475.
- [5] M. Zhu, B. Song, M. Qi, Z. Hu, K. Nomoto, X. Yan, Y. Cao, W. Johnson, E. Kohn, D. Jena, and H. G. Xing, "1.9-kV AlGaIn/GaN Lateral Schottky Barrier Diodes on Silicon," in *IEEE Electron Device Letters*, vol. 36, no. 4, pp. 375-377, April 2015. DOI: 10.1109/LED.2015.2404309.
- [6] J. Gao, M. Wang, R. Yin, S. Liu, C. P. Wen, J. Wang, W. Wu, Y. Hao, Y. Jin, and B. Shen, "Schottky-MOS Hybrid Anode AlGaIn/GaN Lateral Field-Effect Rectifier With Low Onset Voltage and Improved Breakdown Voltage," in *IEEE Electron Device Letters*, vol. 38, no. 10, pp. 1425-1428, Oct. 2017. DOI: 10.1109/LED.2017.2737520.
- [7] J. Ma and E. Matioli, "High-Voltage and Low-Leakage AlGaIn/GaN Tri-Anode Schottky Diodes With Integrated Tri-Gate Transistors," in *IEEE Electron Device Letters*, vol. 38, no. 1, pp. 83-86, Jan. 2017. DOI:

- 10.1109/LED.2016.2632044
- [8] M. Rudan, *Physics of Semiconductor Devices*, 2nd Ed., Springer International Publishing, 2018. DOI: 10.1007/978-3-319-63154-7.
  - [9] B.-S. Wang, G.-Y. Lee, C.-C. Yang, I. Sanyal, and J.-I. Chyi, "Enhancing the Performance of AlGaN/GaN Schottky Barrier Diodes by SF<sub>6</sub> Plasma Treatment and Deep Anode Recess," in *ECS Journal of Solid State Science and Technology*, vol. 6, no. 11, pp. S3081–S3083, Sept. 2017. DOI: 10.1149/2.0081711jss.
  - [10] A. Eblabla, X. Li, I. Thayne, D. J. Wallis, I. Guiney and K. Elgaid, "High Performance GaN High Electron Mobility Transistors on Low Resistivity Silicon for X-Band Applications," in *IEEE Electron Device Letters*, vol. 36, no. 9, pp. 899-901, Sept. 2015. DOI: 10.1109/LED.2015.2460120.